

DETECTION OF SURFACE DISPLACEMENTS AND LIQUEFIED AREAS IN THE 2011 CHRISTCHURCH EARTHQUAKE FROM SAR DATA

Wen Liu^{1*}, Masashi Matsuoka¹, Fumio Yamazaki², Takashi Nonaka³ and Tadashi Sasagawa³

¹ Tokyo Institute of Technology, 4259-G3-2 Nagatsuta, Midori-ku, Yokohama 226-8502 Japan,
liu.w.ad@m.titech.ac.jp; matsuoka.m.ab@m.titech.ac.jp

² Chiba University, 1-33 Yayoi-cho, Inage-ku, Chiba 263-8522, Japan,
fumio.yamazaki@faculty.chiba-u.ac.jp

³ PASCO Corporation, 4-10-1 Nakano, Nakano-Ku, Tokyo, Japan, taakka9299@pasco.co.jp;
taawda5004@pasco.co.jp

*Corresponding author: liu.w.ad@m.titech.ac.jp

ABSTRACT

The Mw 6.1 earthquake affected Christchurch, New Zealand (NZ) on February 21, 2011. It caused widespread damage across the city, especially in the central area. Significant liquefaction occurred widely, which caused ground movement and destroyed lifelines and structures. In this study, the pre- and post-event ALOS/PALSAR and TerraSAR-X (TSX) data are used to detect the ground movements and liquefied areas. Firstly, the differential interferometric analysis (DInSAR) was applied to both the PALSAR and TSX data. The crustal movement caused by the earthquake was estimated by combining the two DInSAR results. Then the coherence value was used to detect the liquefied areas. Intensity images were also introduced to modify the detected result. Finally, the detected liquefied areas were verified by a liquefaction map which was made by field surveys.

Keywords: TerraSAR-X, ALOS/PALSAR, interferometric analysis, coherence, intensity image

INTRODUCTION

The 2011 Christchurch earthquake (Mw 6.1) occurred in the Canterbury region of New Zealand's South Island on February 22, 2011. The epicenter was 6 km away from Christchurch, which is the second-most populous city in New Zealand. The Christchurch earthquake was one of the aftershocks of the Mw 7.0 Darfield earthquake on September 2, 2010 [1]. More than 180 people were killed and 100 thousands buildings were destroyed during the earthquake [2]. Significant liquefaction occurred and produced about 400 thousands tones of slit, which was reported worse than the 2010 Darfield earthquake. According to the field observations carried by Cubrinovski *et al.* [3], the liquefied area in the eastern Christchurch was about 35 km².

Since liquefaction usually causes structural and lifeline damages, mapping it quickly after the earthquake is an important issue for emergency response. However, field-based mapping is laborious and costs time. In addition, it becomes difficult when liquefied areas are inaccessible or covering a large territory. Thus, detecting liquefaction from satellite images is considered to be a useful and power tool. There has been many researches to detect damages due to earthquakes from optical and synthetic aperture radar (SAR) images [4-6]. Oommen *et al.* [7] proposed an alternate method using Landsat ETM+ images to identify liquefaction in Kutch region, India. Due to the weather condition, optical images are not always available after an earthquake. Atzori *et al.* [8] showed the relationship between the reduction of coherence and the occurrence of liquefaction using COSMO-SkyMed data. Ishitsuka *et al.* [9] demonstrated liquefaction occurred along the Tokyo Bay and the Tone River after the 2011 Tohoku-Oki earthquake using the coherence from ALOS/PALSAR data. However, these methods need more than two pre-event and one post-event SAR data.

In this study, we firstly detected the displacements caused by the 2011 Christchurch earthquake from an DInSAR analysis using both the pre- and post-event PALSAR and TerraSAR-X (TSX) data. Then the two-dimensional displacements were estimated by combining these results. The liquefied areas in the central Christchurch were then detected by two methods. The first one is using the coherence and the pre-event intensity images. The areas of low coherence and high backscatter in the pre-event image were considered as the occurrence of liquefaction in built-up areas. The second

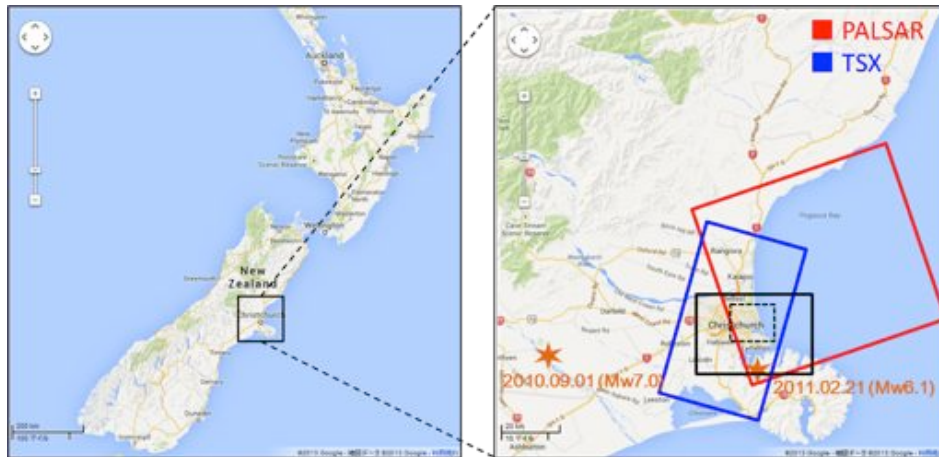


Figure 1 The study area including Christchurch in the east coast of the South Island, New Zealand, which was hit by the Mw 6.1 earthquake on Feb. 21, 2011 (left) and the imaging areas of PALSAR and TerraSAR-X data.

method is from the estimated significant subsidence.

The vertical displacements estimated from the DInSAR analysis were introduced to detect the subsidence caused by liquefaction. Finally, the detected displacements were compared with the GPS data [10]. In addition, the accuracy of the liquefaction detection was compared with a liquefaction map from field observation [3].

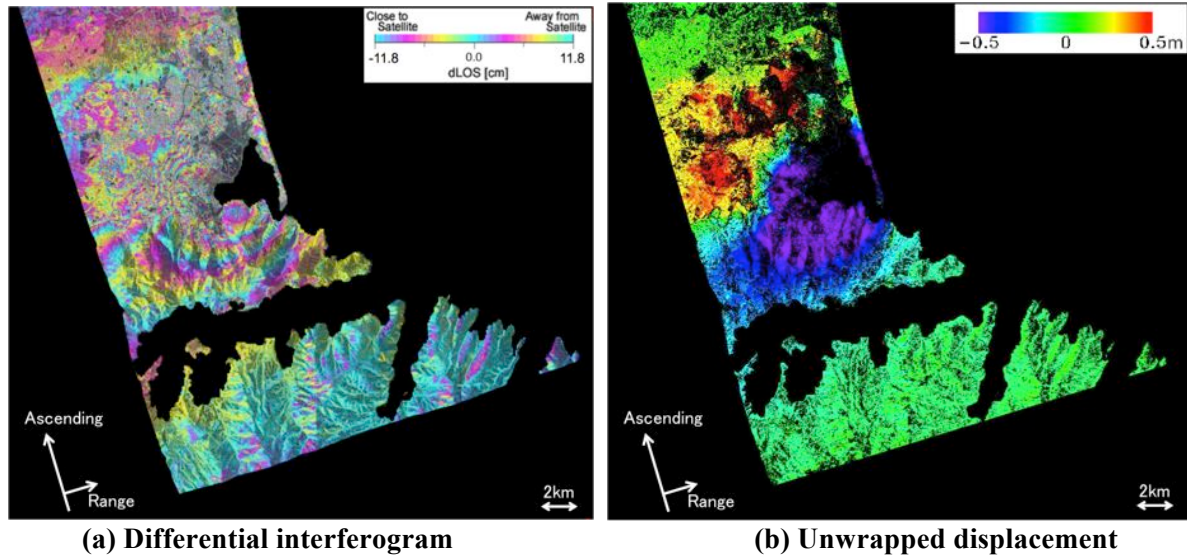
STUDY AREA AND SAR IMAGES

The study area is in the east coast of the South Island of New Zealand, as shown in Figure 1. The pre- and post-event PALSAR and TSX images were used to detect the ground movement and liquefaction. All the images were provided as single look complex data, which include both amplitude and phase information. The pre-event PALSAR image was taken on January 10, 2011 while the post-event one was taken on February 25, 2011, four days after the Christchurch earthquake. The images were taken in the ascending path by the fine beam single (FBS) mode with a 38.95° incidence angle at the center. The normal baseline distance between the two orbits was 363.6 m while the critical baseline for InSAR analysis was 13499.5 m. The time lag was 46 days, one cycle of PALSAR observation. The spatial resolution for the PALSAR images was 4.7 m in the slant range and 3.1 m in the azimuth directions.

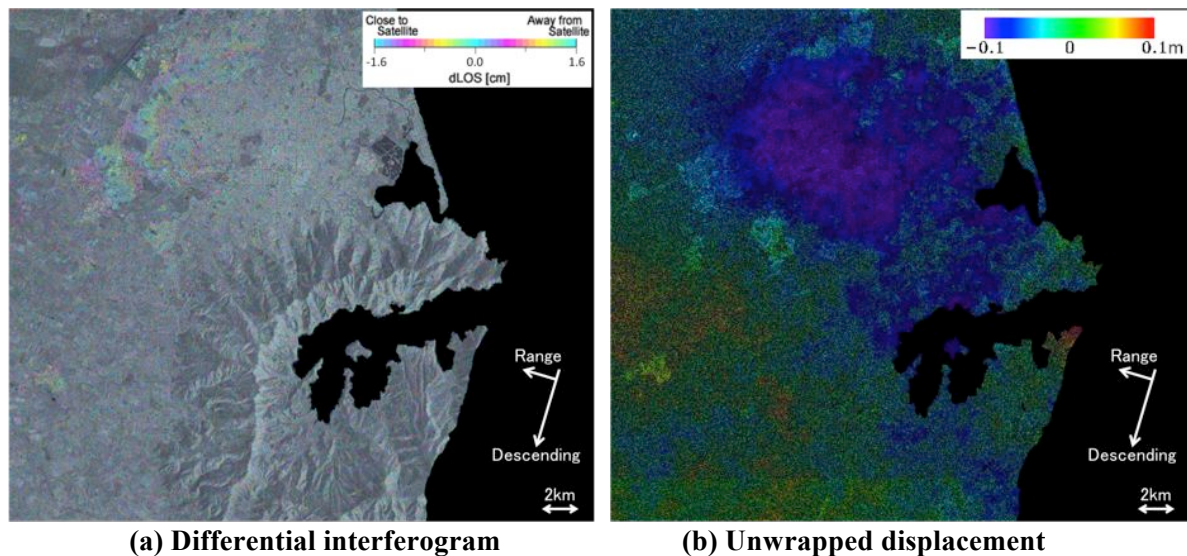
The pre-event TSX image was taken on September 18, 2010 while the post-event one was on March 2, 2011. The TSX images were taken in the descending path by the StripMap mode, with a 44.51° incidence angle at the center. The normal baseline distance for the TSX data was 284.2 m, while the critical baseline was 6290.4 m. The time lag was 165 days, 15 cycles of the TSX's return period. The spatial resolution was 1.4 m in the slant range and 1.9 m in the azimuth directions.

DISPLACEMENTS DETECTION

An InSAR analysis was applied to both the PALSAR and TSX data using ENVI/SARscape software. Firstly, an initial InSAR result which included the orbit fringe, topographic fringe, displacements and noises was calculated from the pre- and post-event SAR data [11]. Then the orbit fringe was removed using the orbit information. A 90 m SRTM DEM in Version 4 was introduced to remove the topographic fringe. The SRTM DEM was downloaded from the website of CGIAR Consortium for Spatial Information (CGIAR-CSI), where the water area has been masked [12]. Then the fringe caused by displacements was obtained by removing noises using a Goldstein filter [13]. In the meantime, the coherence between the two temporal data was also calculated. The window size for coherence estimation is set as 3×3 pixels in both the azimuth and range directions, which was the smallest window size to keep the spatial resolution. Ten ground control points were selected manually around the edge of the data to refine the orbit information and reflate the phases in the interferogram.



(a) Differential interferogram **(b) Unwrapped displacement**
Figure 2 Differential Interferogram (a) obtained from PALSAR data by DInSAR analysis, and the displacements detected by unwrapping the phases (b).



(a) Differential interferogram **(b) Unwrapped displacement**
Figure 3 Differential Interferogram (a) obtained from TSX data by DInSAR analysis, and the displacements detected by unwrapping the phases (b).

Finally, the displacements in the slant range direction could be obtained through the unwrapping process with applying the sensor's wavelength.

The final differential interferogram image from PALSAR data was geo-coded by the SRTM DEM. A part of the imaging area in the black solid frame in Figure 1 was picked up and shown in Figure 2(a). The pixel size was resampled to 10 m. Due to the long wavelength of the L-band and the short time lag, the most of the areas showed high coherence values and a good interferogram was obtained. The significant displacements could be seen around Christchurch City. The big fringes around the south bay were caused by the fault movement while several small circle fringes in the north area were considered as subsidence caused by liquefaction.

The phases with a coherence value larger than 0.5 were unwrapped. Then the displacement in the slant range direction (southwest) was obtained by multiplying with the half wavelength (11.8 cm), and the result is shown in Figure 2(b). The detected displacements were between -1.27 and 1.15 m. The south part of Christchurch City, where the fault moved to the sensor direction due to the earthquake, which means the ground was displaced to the southwest direction or uplifted due the earthquake. However, the displacement close to the fault line could not be detected due to low coherence. The

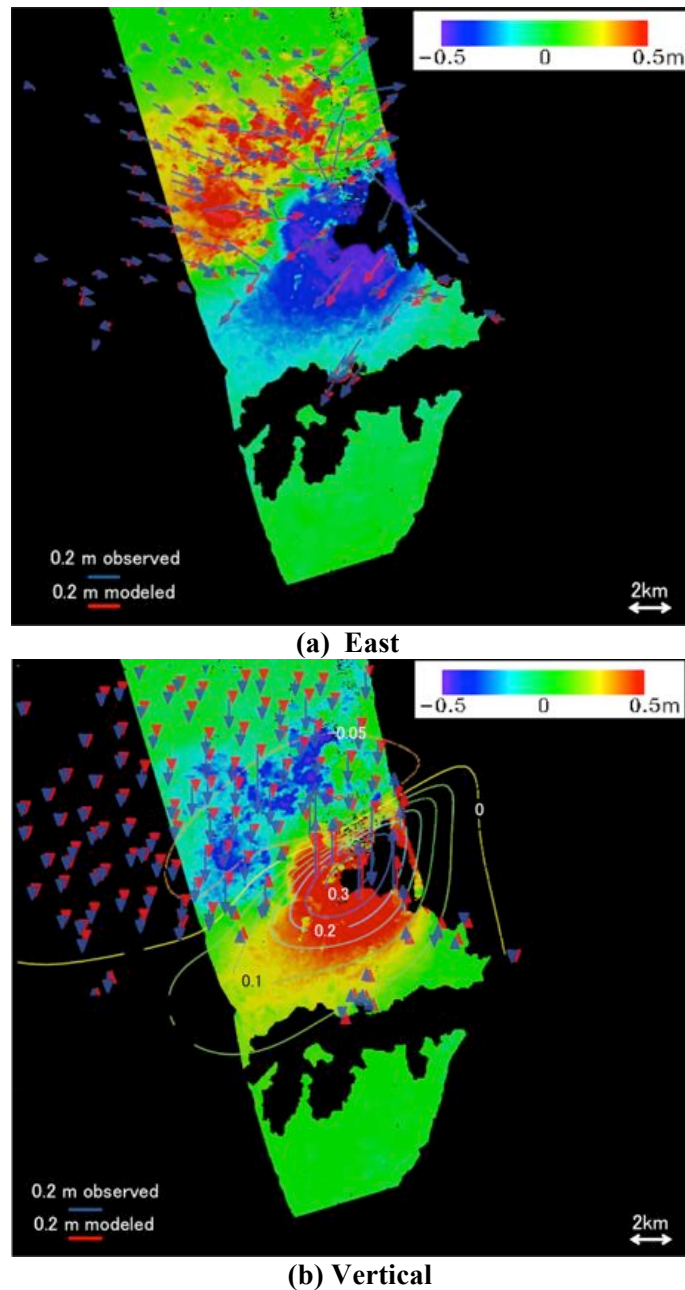


Figure 4 Estimated horizontal movements to the east (a) and the vertical movements (b); Blue arrows (GPS observed data) and red arrows (two-fault model results) were cited from Beaven *et al.* [10].

north part of the city was displaced away from the sensor direction, which means this part moved to the northeast or subsided.

The geo-coded final differential interferogram from the TSX data is shown in Figure 3(a). To match with PALSAR image, the pixel size was also resampled to 10 m. Due to the short wavelength of X-band and the long time lag, the coherence was low in the rural areas. Thus, the fringes in the interferogram were blurry and only shown in the northwestern urban area. However, the fringes with higher coherence than 0.5 were unwrapped and transformed into the displacement. The geo-coded displacement image is shown in Figure 3(b), which is between -0.20 and 0.12 m, much smaller than the results from the PALSAR data. The northwestern urban area with high coherence was seen to move to the sensor direction, which means the ground was displaced to the southeast or uplifted after the earthquake. The fault area which was detected as moving to the southwest from the PALSAR data was also shown as minus values. According to the GPS observation shown in Figure 4 [10], the horizontal movements to the southeast in the northern area were canceled out by subsidence. In

addition, the movements in the southern area, which moved to the southwest direction, were canceled out by the rising. Thus, the detected movements from the TSX data were smaller than these from the PALSAR data. However, the both results were matched with the trend of the GPS observed data. Depending on these trends, the ascending data was considered to be more suitable than the descending data to grasp the characteristics of crustal movements in this earthquake.

The surface displacement is a vector in the three-dimensional space with three components, D_E , D_N , and D_Z , to the east, north, and vertical directions, respectively. DInSAR analysis can detect only the slant range displacement. The relationship between an actual 3D crustal movement and its shift in the slant range is represented by (1).

$$M_r = (D_E \cos \alpha - D_N \sin \alpha) \cos \theta - D_Z \sin \theta \quad (1)$$

where M_r is the shift in the SAR image; α is the heading angle clockwise from the north; and θ is the SAR incident angle.

Since the PALSAR and TSX data were acquired from the different paths, two equations can be built using the detected results. According to the orbits' heading angles, the multiplier for D_N is very small. Thus, the effect of D_N on M_r was negligible. Then D_E and D_Z were calculated from two DInSAR results. The estimated displacements to the east and vertical directions were shown in Figure 4. A low pass filter with 9 x 9 pixels was applied to cover several no-data areas. The horizontal movements were between -0.9 and 0.9 m, and the vertical movements were between -0.7 and 0.9 m. According to the results, the north part of Christchurch moved to the east and subsided, while the south part moved to the west and rose. The GPS observation data cited from Beaven *et al.* [10] is also shown in Figure 4 by blue arrows, while the result by a two-fault model is shown by red arrows. The trends of the horizontal and vertical movements were matched with both the GPS data and arrows. In addition, the boundary of movements was also matched with the model. According to the fault model, the north part subsided homogeneously. However, our estimated results and several GPS data showed larger subsidence in the some areas. These significant subsidence was considered to be caused by the liquefaction. More qualitative comparison cannot be carried since we do not have detail data. However, our estimated results seem to be a little bit larger than the GPS data. Since we disregard D_N in the estimation, the D_N values, if existed, were converted into D_E and D_Z Components. Thus the estimated results in the east and vertical directions might be evaluated larger than they should be.

LIQUEFACTION DETECTION

The 2010 Darfiled and 2011 Christchurch earthquakes caused widespread liquefaction in the suburbs of Christchurch and its residential district. The liquefaction caused the damage to residential buildings and lifelines. The central Christchurch shown in the black dotted frame in Figure 1 was picked up in this study, to estimate liquefied areas. Atzori *et al.* [8] and Ishitsuka *et al.* [9] have proposed the methods to detect liquefaction using the difference between preseismic and coseismic coherence values. In this study, we attempted to detect liquefaction using the coseismic coherence and pre-event backscattering coefficient.

A color composite of the pre-event PALSAR's backscattering coefficient and coherence is shown in Figure 5(a). The pre-event intensity image was processed from the complex data by multi-looking, radiometric calibration and geo-coding processes, and shown in a red band. The geo-coded intensity image was from -33 to 24 dB, and resampled as 6.25 m/pixel. To match with the intensity image, the coherence image was also resampled as the same pixel size, shown in green and blue bands. The red area in Figure 5(a) was regarded as liquefied areas, which have low coherence and high backscattering coefficients. The reasons for the low coherence can be counted as temporal decorrelation and land surface changes. The temporal decorrelation primarily occurred in vegetated areas, which have lower backscatter than urban land-cover. Thus, vegetation can be removed by introducing a pre-event intensity image.

The red area in Figure 5(a) was extracted by segmentation and filtering. Firstly, a low pass filter was applied to both the coherence and pre-event intensity images. The window size was set as 9 x 9 pixels, which is equal to about 50 x 50 m. Two threshold values were set by visual comparison. For the coherence image, the threshold value was determined as 0.54 while it was set as -18 dB for the pre-event intensity image. The pixels with lower coherence than 0.54 and higher intensity than -18 dB

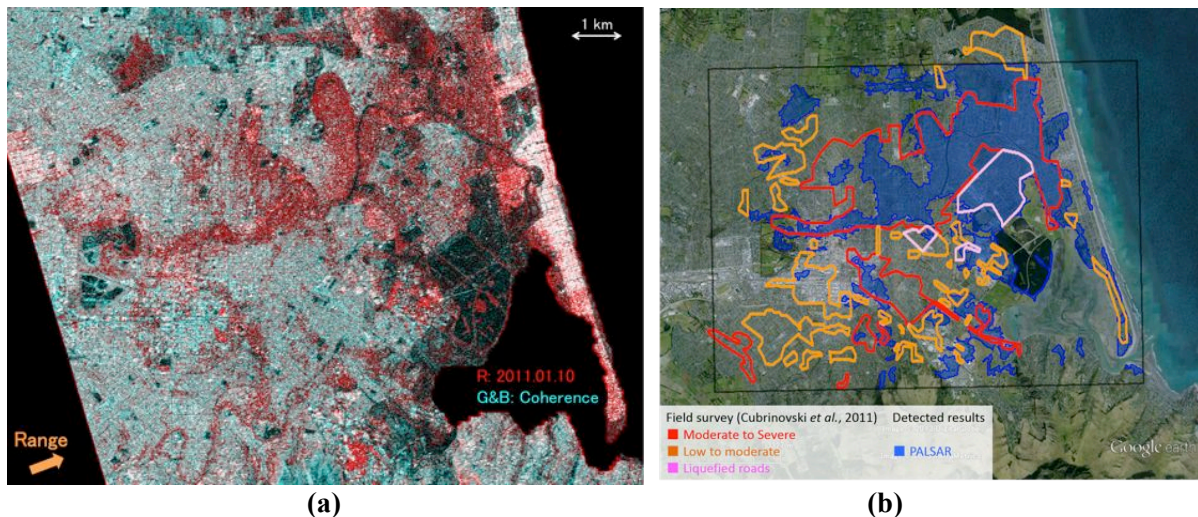


Figure 5 Color composites of the pre-event intensity image and coherence in the central Christchurch (a); comparison of the liquefaction map [3] and the detected liquefaction by low coherence and high backscatter before the earthquake (b).

in the pre-event image were grouped into objects. The objects which were larger than 1000 pixel (about 0.04 km²) were extracted as liquefaction. Then the holes located completely inside of the objects were filled to improve the results. The final result is shown in Figure 5(b) by blue polygons. Comparing with the liquefaction map made by Cubrinovsk *et al.* [3] shown in red, yellow and pink polygons, the most of severe liquefaction areas were matched with our extracted results. In addition, liquefaction of roads were also extracted successfully by our method. A detailed comparison in a pixel-base is shown in Table 1(a). 60% of severe liquefaction and 87% of liquefied roads were extracted. Only 13% of moderate liquefaction was extracted successfully. The producer accuracy for liquefaction was 50% and the user accuracy was 58%. The overall accuracy was 77%. Since the liquefied roads had significant changes on their surface, the coherence was low and could be extracted. The low accuracy for moderate liquefaction could be considered as less changes on the surface. Thus, the extraction using the coherence depends on the surface changes.

A pickup of the vertical displacements detected in the previous section is shown in Figure 6(a). Comparing with the liquefaction map, the detected subsidence seem to be related with liquefaction. Thus, we also attempt to extract liquefaction from the vertical displacement. According to the fault model shown in Figure 4(b), the subsidence in the north part should be 0.05 m. However, our detected displacements were larger than the GPS data and the model. Thus, the threshold value was set as -0.2 m. The areas with the subsidence larger than 0.2 m was extracted as liquefaction. The extracted pixels were grouped into objects, and the enclosed holes were filled. The objects larger than 1000 pixels were regarded as the final result, and shown in Figure 6(b) by magenta polygons.

A comparison of the extracted liquefied areas and the liquefaction map is shown in Table 1(b). 49% of severely liquefied areas were extracted successfully, and 40% of moderately liquefied area were extracted. Comparing with the accuracy of the detection from coherence, the accuracy for severe liquefaction was a little bit lower but that for moderate liquefaction was higher. It seems that moderate liquefaction without surface change but subsided could be extracted by this method. However, the liquefied road is difficult to extract from subsidence. The producer accuracy for all the liquefaction categories (including severe, moderate and road) was 43% and the user accuracy was 68%. The overall accuracy for the extraction is 79%, a litter higher than that from coherence. Since not all the liquefied areas subsided, the produce accuracy for all liquefaction is smaller than that from coherence, especially for severe liquefaction.

CONCLUSION

In this study, the surface displacements caused by the 2011 Christchurch earthquake were detected by combining DInSAR results from pre- and post-event ALOS/PALSAR and TerraSAR-X data. The slant range movements in the ascending and the descending paths were detected from

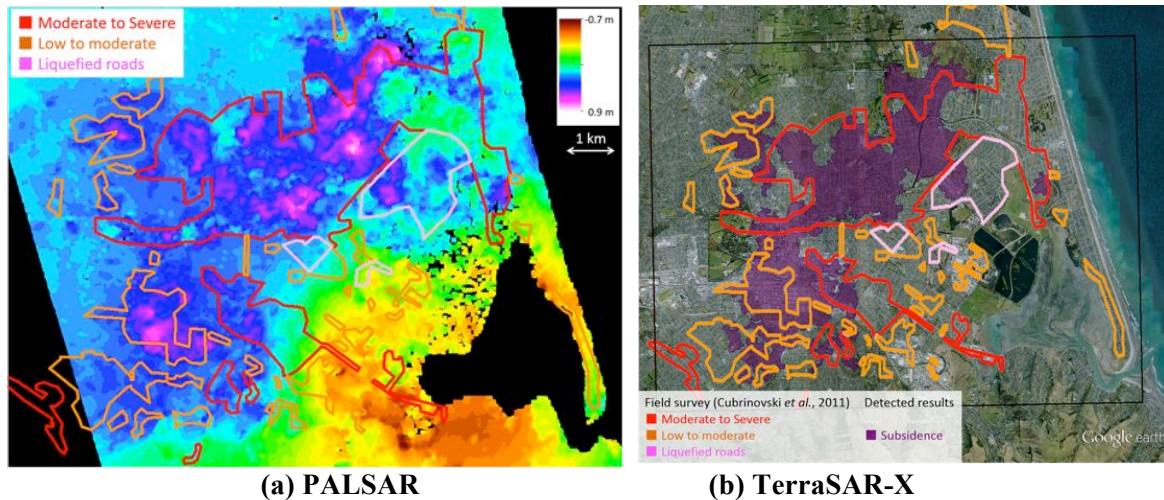


Figure 6 Comparison between the liquefaction map [3] and the estimated vertical displacements (a); the detected subsidence and the liquefaction map overlapping on Google earth (b).

Table 1 Accuracy (%) of detected liquefaction from the coherence (a) and the vertical displacement (b), compared with the liquefaction map [3].

(a)

From Coherence		Field survey results					
		Liquefaction			No liquefaction	Total	User accuracy
		Severe	Moderate	Road			
PALSAR data	Liquefaction	10.04	0.90	2.28	9.64	22.86	57.83
	No liquefaction	6.79	6.20	0.36	63.78	77.14	82.69
	Total	16.83	7.10	2.64	73.43	100.00	
	Producer accuracy	59.66	12.68	86.40	86.87		77.01

(b)

From Vertical displacement		Field survey results					
		Liquefaction			No liquefaction	Total	User accuracy
		Severe	Moderate	Road			
Subsidence	Liquefaction	8.24	2.85	0.40	5.43	16.92	67.89
	No liquefaction	8.61	4.24	2.23	68.00	83.08	81.85
	Total	16.85	7.09	2.63	73.43	100.00	
	Producer accuracy	48.89	40.17	15.30	92.60		79.49

PALSAR and TSX data, respectively. Then the horizontal movements to the east and the vertical movements were estimated by combining the two detected results. Comparing with the GPS observed data and the two-faults model built by Beaven *et al.* [10], our estimated results were a little larger than those. However, the boundary of the fault and the trends of crustal movement were in good agreement with them.

In addition, the extraction of liquefaction was carried out using the PALSAR's coherence and the detected subsidence. By introducing the pre-event backscattering coefficients, the temporal decorrelation for vegetated areas could be excluded. Comparing with the liquefaction map made by the field survey [3], the overall accuracy for our extraction was 77%. More than half of severe liquefaction and 80% of liquefied roads were extracted successfully. However, moderate liquefaction could not be extracted using coherence. Thus, a detection using subsidence was carried out. The vertical movement estimated by the InSAR analysis was introduced to detect liquefaction. Comparing with the liquefaction map, liquefied roads were difficult to extract. However, 40% of moderately liquefied areas was extracted and the overall accuracy for the extraction was 79%. Due to the different characteristics of the extraction methods, it seems possible to classify the level of liquefaction by combining the both results in the future.

ACKNOWLEDGMENT

PALSAR data are owned by the Ministry of Economy, Trade and Industry (METI) and Japan Aerospace Exploration Agency (JAXA). TerraSAR-X data are the property of German Aerospace Center (DLR) and the Inforterra GmbH, and provided by PASCO Corporation. This study was supported in part by a grant in aid for scientific research (Research No. 25003050 and 25282117; Principal Investigator: Masashi Matsuoka, Research No. 21310119; Principal Investigator: Fumio Yamazaki). We would like to express our gratitude for these contributions.

REFERENCES

- [1] Gledhill, K., Ristau, J., Reyners, M., Fry, B., Holden C., 2011, The Darfield (Canterbury, New Zealand) Mw 7.1 earthquake of September 2010: A preliminary seismological report, *Seismological Research Letters*, 82(3) 378-386.
- [2] New Zealand Police, 2012: <http://www.police.govt.nz/major-events/previous-major-events/christchurch-earthquake/list-deceased> (accessed on 21st August, 2013).
- [3] Cubrinovshi, M., Bray, J. D., Taylor, M., Giorgini, S., Bradley, B., Wotherspoon, L., Zupan, J., 2011, Soil liquefaction effects in the central business district during the February 2011 Christchurch earthquake, *Seismological Research Letters*, 82(6) 893-904.
- [4] Matsuoka, M., Yamazaki, F., 2004, Use of satellite SAR intensity imagery for detecting building areas damaged due to earthquakes, *Earthquake Spectra*, (20) 975-994.
- [5] Huyck, C., Adams, B., Cho, S., Chung, H. C., Eguchi, R., 2005, Towards rapid citywide damage mapping using neighborhood edge dissimilarities in very high-resolution optical satellite imagery-application to the 2003 Bam, Iran earthquake, *Earthquake Spectra*, 21(S1) 255-266.
- [6] Stramonodo, S., Bignami, C., Chini, M., Pierdicca N., Tertulliani A., 2006, Satellite radar and optical remote sensing for earthquake damage detection: results from different case studies, *International Journal of Remote Sensing*, (27) 4433-4447.
- [7] Oommen, T., Baise, L. G., Gens, R., Prakash, A., Gupta, R. P., 2010, Documenting liquefaction failures using satellite remote sensing, *8th International Workshop on Remote Sensing for Disaster Management*, Tokyo, Japan. Available: <https://mceer.buffalo.edu/publications/workshop/RS-8/default.asp> (accessed on 21st August, 2013).
- [8] Atzori, S., Tolomei, C., Antonioli, A., Merryman Boncori, J. P., Bannister, S., Trasatti, E., Pasquail P., Salvi, S., 2012, The 2010-2011 Canterbury, New Zealand, seismic sequence: Multiple source analysis from InSAR data and modeling, *Journal of Geophysical Research*, (117) B080305.
- [9] Ishituska, K., Tsuji, T., Matsuoka, T., 2012, Detection and mapping of soil liquefaction in the 2011 Tohoku earthquake using SAR interferometry, *Earth Planets Space*, (64) 1267-1276.
- [10] Beaven, J., Fielding, E., Motagh, M., Samsonov, S., Nonnelly, N., 2011, Fault location and slip distribution of the 22 February 2011 Mw 6.2 Christchurch, New Zealand, earthquake from geodetic data, *Seismological Research Letters*, 82(6) 789-799.
- [11] Monti Guarnieri, A., Gussione, P., Pasquali P., Desnos, Y.-L., 2003, Multi-mode ENVISAT ASAR interferometry: techniques and preliminary results, Radar, Sonar and Navigation, *IEEE Proceedings*, 150(3) 193-200.
- [12] CGIAR CSI, 2004: <http://www.cgiar-csi.org/data/srtm-90m-digital-elevation-database-v4-1#download> (accessed on 21st August, 2013).
- [13] Goldstein R. M., Werner, C. L. m 1997, Radar ice motion interferometry, *Third ERS Symposium on Space at the service of our Environment*, (2) 969-972, Florence, Italy.